

Kinetics-Optimized Enhanced Sampling Using Mean First Passage Times

Tiejun Wei¹, Balint Dudas¹, and Edina Rosta¹

¹*University College London, Department of Physics and Astronomy
London WC1E 6BS*

Correspondence: e.rosta@ucl.ac.uk

Molecular dynamics simulations have become essential in many areas of atomistic modelling from drug discovery to materials science. They provide critical atomic-level insights into key dynamical events experiments cannot easily capture. However, their impact often falls short as the timescales of the important processes are inaccessible using standard molecular dynamics. Enhanced sampling methods provided avenues to access such crucial rare events, for example key slow conformational changes of biomolecules. However, the bias in enhanced sampling simulations is rarely optimized, and even if they are, the optimization criteria is based on the thermodynamics or Hamiltonian of the system, but do not directly consider molecular kinetics. Here, we introduce a novel enhanced sampling algorithm that adaptively optimizes the bias based on the kinetics of the system for the first time. We identify the optimal bias that minimizes a key physical observable, the mean first passage time (MFPT) from a starting state to a target state. Our algorithm makes use of the relation between biased and unbiased kinetics obtained from discretized Markov state models (MSMs), as established in the dynamic histogram analysis method (DHAM). We demonstrate the applicability of the method for different 1D and 2D analytical potential-based model examples, NaCl dissociation in explicit water, and phosphate unbinding in Ras GTPase. Our algorithm has excellent performance compared with state-of-art enhanced sampling methods in terms of the timescales required to reach the final state in the benchmarking systems. Our findings provide a novel, kinetics-driven enhanced sampling strategy, signatured by a targeted approach to facilitate mapping rare events, with the potential for breakthrough applications in drug discovery and materials science.

Keywords: Markov State Models, enhanced sampling, biased molecular dynamics, molecular kinetics

I. INTRODUCTION

Biomolecular simulations, including all atom molecular dynamics (MD) have become essential to provide unprecedented details into the dynamics of complex systems. In particular, slow conformational changes in biomolecular systems play a crucial role in many biological functions, but are mostly unavailable experimentally, particularly the atomic level insights into the rate limiting transition states and corresponding mechanistic pathways. MD simulations therefore find key applications in e.g., drug discovery, as powerful tools to provide important structural and energetic information for complex systems of biomedical interest [1,2]. On the other hand, their impact often falls short due to the well-known sampling problem [3,4]. While aiming to uncover pivotal rare events, these simulations frequently stall in local minima, consuming extensive computational resources, limiting the timescales that can be reached to study biomolecular processes.

Enhanced sampling algorithms are developed to overcome this dilemma, and access orders of magnitude longer timescales that would be beyond reach for current computational resources [5]. A wide variety of simulation strategies were proposed to map pathways from an initial state based on adding a bias to the Hamiltonian of the system. Beyond the classical umbrella sampling (US) [6], adaptive methods such as the finite temperature string method [7], its

variant with coupled Hamiltonian replica exchange method [8], targeted MD [9], milestone-based sampling [10], Adaptive Biasing Force [11,12], as well as metadynamics (MetaD) and its improved variants, well-tempered metadynamics (WT-MetaD) [13–15] were successful to explore the conformational space by deploying and optimizing bias [16].

In most of biasing strategies, thermodynamics-based bias is applied to the system. For example, MetaD aims to explore the selected collective variable (CV) space and iteratively identify the bias that, when added to the original Hamiltonian, provides a flat surface [13]. WT-MetaD includes additional parameters to enable a smooth biasing process [15]. Additionally, machine learning-aided enhanced sampling methods are also gaining attention as promising avenue for CV selection and sampling [17–21]. However, these algorithms are not directly optimal to reduce the timescale for the conformational change of interest, and the bias is not optimized for the underlying molecular kinetics.

To describe the underlying molecular kinetics of the system, Markov state models (MSM) were highly successful [3,22,23]. These also find applications in both deep learning and reinforcement learning strategies, such as using the multi-armed bandit framework [24] or autoencoders [25]. Alternatively, transition path sampling (TPS) methods [26–28] and finite temperature string method [7] also provide valuable insights into the kinetics of

rare events [10,28,29]. However, the lack of bias in these methods limits the timescales that can be reached [30].

To design optimal kinetics-based bias, an analytical relationship is needed between the dynamics of the biased and unbiased systems. However, the weighted histogram analysis method (WHAM) [31], which is typically used to estimate the unbiased free energy profiles from biased runs, does not provide kinetic information. To enable the estimation of the unbiased kinetics, the recently developed dynamic histogram analysis method (DHAM) [22] provides the necessary theoretical framework to build the unbiased MSM from multiple biased trajectories. The DHAM and its extension to rate matrices (DHAMed) [32] were developed to yield unbiased rates/Markov matrices, as well as the free energy surface (FES).

Here, we propose a novel enhanced sampling algorithm that identifies the optimal bias to reach the target state from an initial starting state. We use the mean first passage time (MFPT) as a key quantity that measures the time required for the transition pathway as our optimization criterium [33–35]. We formulate an optimization problem, where the bias is defined as the summation of a set of Gaussian functions (see SI.2.), with the underlying parameters optimized to minimize the MFPT from the starting state to the target state. We demonstrate that such optimal biased potential leads to an overall Hamiltonian corresponding to downhill trajectories in analytical examples. We also provide examples of all atom MD simulations of a solvated NaCl ion pair and Ras-Ras GTPase-activating protein (Ras.GAP) complex system [36] to benchmark the performance of the proposed algorithm with WT-MetaD and classical MD.

II. MARKOV STATE MODELS AND MEAN FIRST PASSAGE TIMES

The MSM model serves as a quantitative tool to analyze the dynamics of the system as a Markov chain. It is common to use discrete states to represent different conformational clusters of the system. The transition between the states can be explicitly expressed by a rate matrix \mathbf{K} , or a transition probability matrix, \mathbf{M} , the Markov matrix. The rate matrix \mathbf{K} contains the transition probabilities per unit time. In the context of continuous time, it describes the progress of an initial population at time 0, $\mathbf{p}(0) \in [0,1]^n$ to the population after a lag time t :

$$\mathbf{p}(t) = e^{\mathbf{K}t} \mathbf{p}(0) \quad (1)$$

where $\mathbf{p}(t)$ represents the population of n discrete states at time t . The corresponding transition probability matrix or Markov matrix for lag time t is defined as $\mathbf{M} = e^{\mathbf{K}t}$. A key kinetic quantity of the system is the MFPT matrix, which provides a measure of how quickly the system reaches the target state j starting from state i . [35,37]. The MFPT

matrix can be calculated from \mathbf{K} (or analogously from \mathbf{M}) as:

$$t_{ji} = \frac{1}{p_j^{\text{eq}}} [(\mathbf{p}^{\text{eq}} \mathbf{1}_n^T - \mathbf{K})_{jj}^{-1} - (\mathbf{p}^{\text{eq}} \mathbf{1}_n^T - \mathbf{K})_{ji}^{-1}] \quad (2)$$

where t_{ji} represents the MFPT from state i to state j , p_j^{eq} stands for the equilibrium probability of state $j \in \{1, \dots, n\}$ with shape of $[n, 1]$, and $\mathbf{1}_n^T$ is an all-ones row vector. Eq. (2) quantifies the average time it takes for the system to first reach state j , starting from state i [37].

The aim is to identify the best u^* bias that would provide an optimal biased rate matrix, $\mathbf{K}_{bias}^{\alpha}$, which minimizes t_{fs} MFPT given a starting state, s , to the final state, f , note that $s, f \in \{1, \dots, n\}$. We envision that the optimal bias is determined iteratively based on the current sampling history, to allow progressive exploration of the phase space over several iterations, α . We introduced a relation between unbiased and biased rate or Markov matrices [22], such that the ji -th element of a biased rate matrix $\mathbf{K}_{bias}^{\alpha}$ and unbiased rate matrix \mathbf{K} have the following relationship:

$$\frac{k_{ji}^{\alpha}}{k_{ji}} \propto \exp\left(-\frac{u_j^{\alpha} - u_i^{\alpha}}{2k_B T}\right) \quad (3)$$

where u_i^{α} is the bias for state i in iteration α , k_B is the Boltzmann constant, and T is the temperature of the simulation. For the Markov matrix ($\mathbf{M}_{bias}^{\alpha}$) the analogous relation holds for short lag time with good approximation [38].

We consider the system with its Hamiltonian $H = U(\mathbf{x})$, where $\mathbf{x} \in \mathbb{R}^{3N}$ represents the 3D coordinates of the N atoms of the system, and U represents the overall potential energy. We define a Markov transition probability matrix typically in a reduced space, via a d -dimensional CV space: $\xi(\mathbf{x}) \in \mathbb{R}^d$.

As bias, in this work we use a sum of N_{gauss} Gaussian functions in the CV space $\xi(\mathbf{x})$, with the i -th Gaussian kernel G_i^{α} centered at μ_i^{α} , with amplitude A_i^{α} and width σ_i^{α} , such that:

$$u_{bias}^{\alpha}(\xi) = \sum_{i=1}^{N_{gauss}} G_i^{\alpha}(\mu_i^{\alpha}, A_i^{\alpha}, \sigma_i^{\alpha}; \xi) \quad (4)$$

The Gaussian parameters ($\mu_i^{\alpha}, A_i^{\alpha}, \sigma_i^{\alpha}$) can then be optimized such that they yield the minimal MFPT value t_{fs} from the starting state s , to the final state f . The search for the optimal bias u_{bias}^{α} of the system is a simple minimization problem as defined below:

$$u_{bias}^\alpha = \operatorname{argmin}_{U_{bias}(\xi)} \{ \text{MFPT}(\mathbf{x}_s \rightarrow \mathbf{x}_f) | \mathbf{K} \} \quad (5)$$

where we optimize all $\mu_i^\alpha, A_i^\alpha, \sigma_i^\alpha, i = 1, \dots, N_{gauss}$ parameters for a given unbiased rate matrix \mathbf{K} to minimize the mean first passage time t_{fs} , where f and s are the bins that correspond to positions $\xi(\mathbf{x}_f)$ and $\xi(\mathbf{x}_s)$, respectively.

In most applications, the FES of the system is *a priori* unknown, therefore the kinetic information needed to construct a Markov matrix has to be collected from simulation data. Starting from initially unbiased simulations, we can iteratively update the Markov matrix of the system as well as the optimal bias. We start with $u_{bias}^\alpha(\xi(\mathbf{x})) = 0$ at iteration $\alpha = 0$, yielding a new trajectory $\mathbf{x}^\alpha(t)$, $t = 0, \dots, T_{max}$ of length T_{max} , where the coordinates \mathbf{x} of the system are recorded and the corresponding CV, $\xi(\mathbf{x})$ is calculated. We iteratively update the estimated Markov matrix using the DHAM algorithm given all the α trajectories, $\xi^i(t), i = 0, \dots, \alpha$, and their corresponding bias [22]. This is achieved by unbiasing all the trajectories $\mathbf{x}^i(t)$ with sets of biasing potentials $u_{bias}^i(\xi)$ used throughout all iterations $i = 0, \dots, \alpha$, and obtaining an estimated Markov matrix \mathbf{M}_{est}^α .

However, during most propagation steps, prior to reaching the *global target state* \mathbf{x}_f , the estimated Markov matrix \mathbf{M}_{est}^α does not hold the kinetic information linking any state to this global target. To address this, we introduced intermediate target states, termed a *local target state* \mathbf{x}'_f , to guide the optimization of biasing potentials. The local target is defined as the state most proximate to the *global target state* within the explored CV space. Note that if we have recorded the transition linking any state to the *global target state*, we will have $\mathbf{x}_f = \mathbf{x}'_f$.

We then find the new set of Gaussian kernel parameters ($\mu_i^{\alpha+1}, A_i^{\alpha+1}, \sigma_i^{\alpha+1}, i = 0, \dots, N_{gauss}$) that constitute the bias $G_i^{\alpha+1}$ for the next iteration ($\alpha + 1$) with the bias potential $u_{bias}^{\alpha+1}(\xi)$. Note that we search this by minimizing the biased MFPT from the last position, $\mathbf{x}^\alpha(T_{max})$ to the *local target state* \mathbf{x}'_f :

$$u_{bias}^{\alpha+1} = \operatorname{argmin}_{U_{bias}(\xi)} \{ \text{MFPT}(\mathbf{x}^\alpha(T_{max}) \rightarrow \mathbf{x}'_f) | \mathbf{M}_{est}^\alpha \} \quad (6)$$

The proposed novel enhanced sampling algorithm, termed as KOMBI (Kinetics-Optimized Markovian Bias Integration), can be summarized as the pseudo code in Algorithm 1.

Algorithm 1. KOMBI CV Space Exploration

0: **procedure** KOMBI enhanced sampling

1: Initialize the simulation system with $H = U(\mathbf{x})$ and a starting state $\mathbf{x}^\alpha(0)$ for $\alpha = 0$.

2: Define global target state \mathbf{x}_f and convergence threshold δ .

3: Initialize Gaussian parameters for the initial biasing potential. $u_{bias}^\alpha(\xi) = 0$ for $\alpha = 0$.

4: **for** $\alpha = 1$ to Maxiter **do**:

5: Perform MD with $H = U(\mathbf{x}) + u_{bias}^\alpha(\xi)$.

6: Obtain trajectory $\mathbf{x}^\alpha(t)$ of length T_{max} .

7: **if** ($|\mathbf{x} - \mathbf{x}_f| < \delta$ for any \mathbf{x} in \mathbf{x}^α):

8: Target reached

9: **break**

10: **end if**

11: Reconstruct the unbiased Markov matrix:

$$\mathbf{M}_{est}^\alpha = \text{DHAM}(\mathbf{x}^i(t), u_{bias}^i(\xi) | i = 0, \dots, \alpha)$$

12: Find optimal bias $u_{bias}^{\alpha+1}(\xi)$ to minimize MFPT to target state:

$$u_{bias}^{\alpha+1} = \operatorname{argmin}_{U_{bias}(\xi)} \{ \text{MFPT}(\mathbf{x}^\alpha(T_{max}) \rightarrow \mathbf{x}'_f) | \mathbf{M}_{est}^\alpha \}.$$

13: **end for**

14: **end procedure**

III. RESULTS

We first demonstrate the algorithm for a 1D model potential-derived rate matrix \mathbf{K} . The original FES is constructed using an analytical potential U (Fig. 1, black line) that is discretized into n states. The transition rates in the unbiased rate matrix are restricted to neighboring states only, where all the non-neighboring transition rate are set to 0:

$$K_{i,i\pm 1} = A \exp\left(\frac{-(U(i\pm 1) - U(i))}{2k_B T}\right) \quad (7)$$

We calculated the optimal bias for different starting states (Fig. 1, symbols) to the target state (green star in Fig. 1a). The results show that the total bias together with the original free energy profile (Fig. 1a, colored lines) yields a downhill

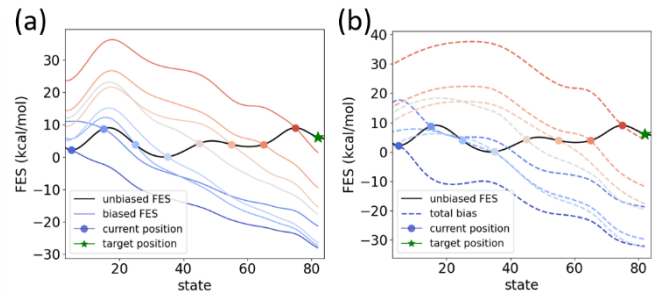


Figure 1. (a) The original FES (black line) with optimized bias (from blue to red) generated for different starting states (circles). (b) The total bias (dashed lines) generated for different starting states (circles). The final state is shown as a green star.

profile from the respective starting points. The optimal bias (Fig. 1b, colored lines) takes up the inverse shape of the original profile with an added slope, ensuring also that the system is unlikely to turn backwards in 1D, further away from the target position, justifying the objective function used as the MFPT: $\text{MFPT}(\mathbf{x}^\alpha(T_{max}) \rightarrow \mathbf{x}_f)$. A 2D example is shown in Fig. 2, indicating that this approach is generalizable to higher dimensions.

We then applied Algorithm 1, assuming that the FES is not known *a priori*, in several benchmarking systems: the 1D model potential (Fig. 1), a 2D model potential (Fig. 2), as well as all atom simulations of solvated NaCl in a box and the dissociation of the cleaved phosphate in Ras.GAP after the GTP hydrolysis step. The simulation details for the benchmarking systems can be found in SI.1-5.

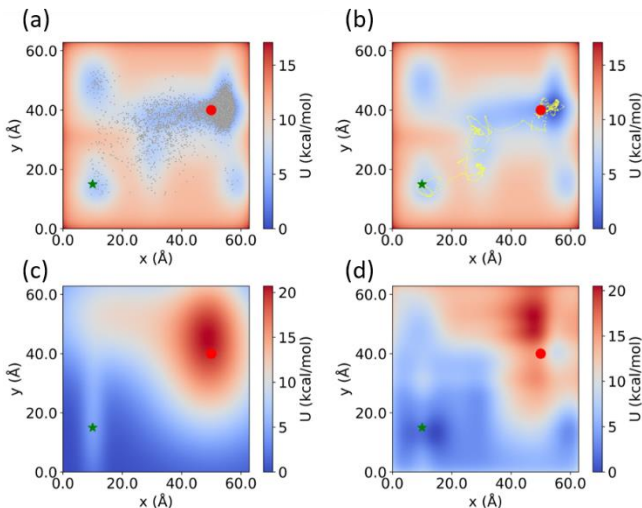


Figure 2. (a-b) Scatter plots of illustrative trajectories for WT-MetaD (a) and for our KOMBI algorithm (b), using a starting position of [50, 40] and target position of [10, 15] on the x-y plane of the 2D free energy surface. Simulation datapoints were taken with time interval of 1 ps. (c) Optimal bias generated using the rate matrix on the 2D surface. (d) Optimally biased overall 2D free energy surface.

For the 1D model potential example, we performed 20 simulations each, using our KOMBI algorithm and MetaD. The system reached the target state (green star, Fig. 1) in $\sim 39 \pm 12.4$ ps in the Langevin dynamics simulations using our MFPT-based adaptive biasing strategy. With WT-MetaD, the system reached the target state in $\sim 34.5 \pm 14.3$ ns (note difference between ns and ps), orders of magnitude slower (as depicted in Fig. 3). We also performed unbiased Langevin dynamics simulations, which took significantly longer to reach the target state than the biased simulations. One long simulation reached the target in $\sim 8.30 \mu\text{s}$ (black cross in Fig. 3, see also Fig. S1). To estimate a MFPT using the analytical potential, we conducted a fitting procedure to

match the prefactor of the analytical model with the diffusion coefficient from the simulated data (for details see SI.3.) and estimated the MFPT needed from the initial state to the final state being $\sim 81.7 \mu\text{s}$ (blue dashed bar in Fig. 3). The KOMBI algorithm demonstrated significant potential in biasing the 1D potential energy surface, achieving several orders of magnitude compared with the classical MD simulations and with the WT-MetaD (Fig. 3).

In the 2D potential energy system (obtained MFPTs are in Fig. 3, grey bars), the KOMBI algorithm showed a more directed, targeted path to reach the target state, reached in $\sim 79.85 \pm 36.42$ ps. The WT-MetaD and classical MD reached the target in $\sim 10.6 \pm 4.1$ ns and $\sim 3.77 \pm 2.3 \mu\text{s}$, respectively. The unbiased MFPT was obtained from three datapoints only (data points shown in Fig. 3, trajectories are illustrated in Fig. S1), and therefore the MFPT was also estimated using our analytical potential and the same prefactor we obtained for the 1D system (SI.3). This resulted an estimated MFPT of $\sim 4.1 \mu\text{s}$ (grey dashed bar, Fig. 3). Notably, the KOMBI method, with a pathway illustrated by a sample trajectory in yellow (Fig. 2b), optimizes the bias in a way that the system is driven towards the target state and is less likely to extensively sample other metastable states. On the other hand, the WT-MetaD (with an example for the sampled region in grey shade in Fig. 2a), exhibits trajectories where the system shows a diffusive and not targeted behaviour exploring the FES below some energy thresholds. Subsequently, the system briefly surveys the entire FES as the energy wells are progressively filled, which is characteristic of the metadynamics sampling.

In the NaCl system, the distance between the ion pair is used as our CV, with an initial distance of 2.5 Å. We define the target state as their distance reaching 8 Å following a rare

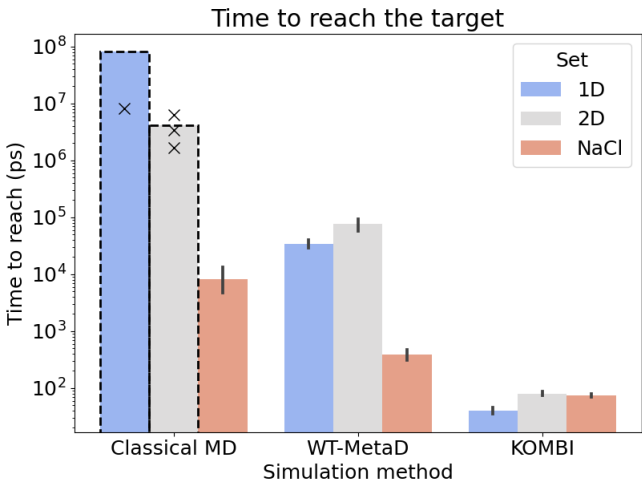


Figure 3. Performance of each simulation method on the 1D/2D potential energy surface, as well as the solvated NaCl system (blue, grey, and red bars, respectively). The bar plots represent the MFPT required to reach the target, with the average and standard error from 20 repeated simulations as error bars. Estimated MFPTs for unbiased, classical MD are shown as dashed bars, with time to reach the target state marked in black cross.

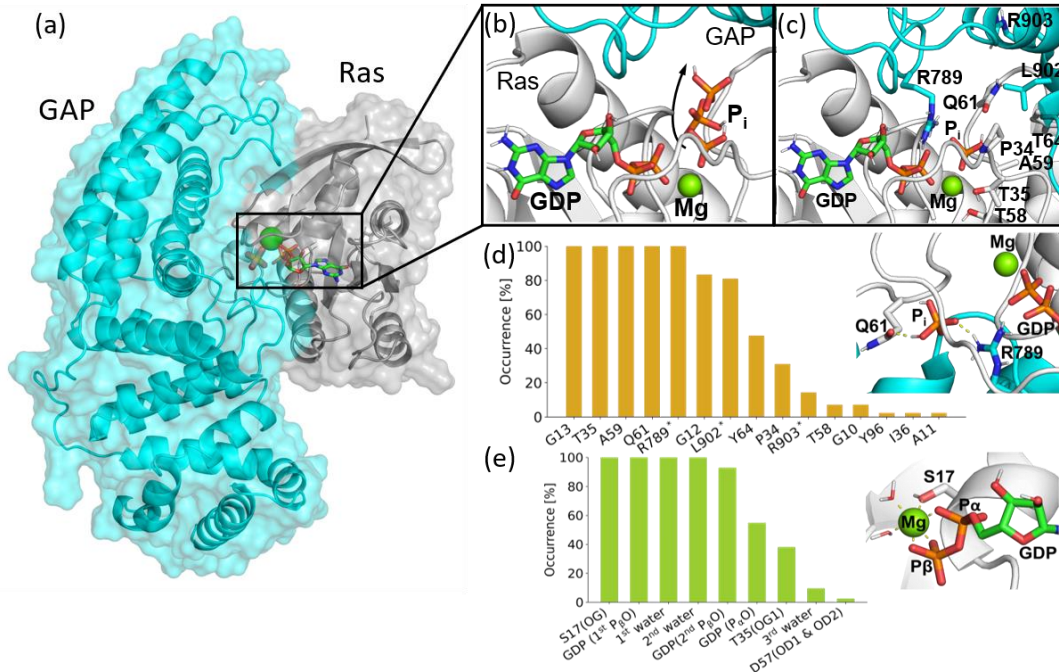


Figure 4. The P_i unbinding path and the rearrangement of the Mg^{2+} coordination sphere during the biased simulations. (a) Schematic overview of the Ras.GAP complex system, water molecules are not shown for clarity. Protein complex (Ras and GAP) is shown in gray, GDP and the $H_2PO_4^-$ ions shown as licorice, Mg^{2+} as a green sphere. (b) Snapshots of the P_i path and (c) residues interacting with the P_i along its unbinding shown in the starting conformation. (d) Residues along the P_i unbinding path showing the proportion of runs in which a given contact was observed (in the bar plot, the residues of GAP are marked by *) and an exemplified stabilized P_i state between $Q61^{Ras}$ and $R789^{GAP}$ residues forming H-bonds. (e) Mg^{2+} -coordinating residues at the end of the unbinding simulations and an example where the Mg^{2+} is shifted to an $\alpha\beta$ -coordinated state.

event, the ion-pair dissociation. This can naturally happen even in the unbiased MD simulations, although it takes $\sim 8.2 \pm 9.8$ ns among 20 trajectories. For the WT-MetaD, the system has seen significant speed-up to mean first passage times of $\sim 387.6 \pm 278.1$ ps. With the KOMBI algorithm, it took $\sim 74.6 \pm 12.2$ ps to disassociate the ion pair. The obtained MFPTs are in Fig. 3 (red bars).

As a more complex and biologically relevant problem, we applied MFPT-based biasing in simulating the phosphate (P_i) unbinding in the Ras.GAP.GDP. P_i complex. The simulations started from the state following the GTP hydrolysis step of the Ras functional cycle. We applied biasing to the distance between the Mg^{2+} and the phosphorus of the P_i . In total, 42 independent simulations were performed. The P_i - Mg^{2+} pair dissociated (the CV reaching 7 Å starting from 3.3 Å) in 793.1 ± 278.3 ps. As a first step, the P_i left the Mg^{2+} coordination sphere. Along its unbinding pathway, the P_i consistently got into close contact with crucial residues of Ras (Q61, A59, T35, and G13) and GAP (R789*) (Fig. 4b, c, d). In addition to $G12^{Ras}$, $Q61^{Ras}$ and $G13^{Ras}$ are the most commonly mutated Ras residues found in cancer whereas $T35^{Ras}$ is conserved in many G domain proteins [39]. $R789^{GAP}$ is an arginine finger residue responsible for the enhanced GTP-hydrolysis [40]. Upon leaving the Mg^{2+} coordination sphere, the P_i is often stabilized between $Q61^{Ras}$ and $R789^{GAP}$ (Fig. 4d).

The adaptation of the Mg^{2+} coordination sphere to the absence of the P_i is also necessary (see also SI.5). The coordination of $T35^{Ras}$ and the P_i is expected to be replaced by two additional water molecules (Fig. S2) [41]. Despite the short simulation time per propagation in our biased simulations, key conformational changes could already be observed. We found that the P_β of GDP, $S17^{Ras}$, and two water molecules coordinate the Mg^{2+} ion during all simulations (Fig. 4e). Interestingly, $T35^{Ras}$, which does not coordinate the Mg^{2+} in the GDP-bound Ras, already left the Mg^{2+} coordination sphere in 62% of our simulations. Due to the lack of available water molecules, a second nonbridging oxygen of the P_β contributed to the Mg^{2+} coordination (93%) and/or the Mg^{2+} shifted to an $\alpha\beta$ -coordinated state (55%) (Fig. 4e).

IV. CONCLUSIONS

In this paper, we propose an MSM-based, kinetics-optimized enhanced sampling algorithm that optimizes the applied bias to minimize the MFPT to a target state. By adaptively updating the bias based on an MSM-based analysis of the discretized phase space using the DHAM method [22], our approach significantly reduces the time required to reach the target states in our test cases. These improvements are demonstrated by orders of magnitude smaller MFPTs for the 1D and 2D analytical potentials and

all-atom simulations of solvated NaCl. Furthermore, our iterative bias generation method facilitates a more direct trajectory from the local starting point to the target state within the phase space, demonstrating that the KOMBI algorithm efficiently directs the system towards the global target without extensive exploration of non-essential directions in the CV space, yet providing a likely pathway. We also provided a practical example using our novel algorithm on the Ras-Ras.GAP system. Structural analysis of the pathways for the phosphate dissociation in the post-ATP-hydrolysis state of the Ras.GAP complex was carried out, with key residues during the unbinding process identified. This underscores the utility of our approach in providing a detailed mechanistic understanding of complex biochemical processes with an ultra-short transition time without distorting the pathways. Our KOMBI algorithm provides a novel, efficient and accurate way to probe conformational changes that normally occur over long timescales using ordinary classical MD simulations. This opens up new ways to explore and facilitate rare events in the selected CV space in a highly-efficient manner, with key applications in drug discovery and materials science.

V. ACKNOWLEDGEMENT

We acknowledge discussions with Alessia Annibale, and valuable input from Dénes Berta. We acknowledge support from ERC (project 757850 BioNet), and EPSRC (grant no. EP/R013012/1). We acknowledge support from the UK Tier 2 HPC clusters and HECBioSim (<http://hecbiosim.ac.uk>). This work used the ARCHER2 UK National Supercomputing Service. This project made use of time on Tier 2 HPC facility JADE, funded by EPSRC (EP/P020275/1).

-
- [1] K. Ahmad, A. Rizzi, R. Capelli, D. Mandelli, W. Lyu, and P. Carloni, *Enhanced-Sampling Simulations for the Estimation of Ligand Binding Kinetics: Current Status and Perspective*, *Front Mol Biosci* **9**, (2022).
- [2] D. J. Huggins et al., *Biomolecular Simulations: From Dynamics and Mechanisms to Computational Assays of Biological Activity*, *WIREs Computational Molecular Science* **9**, (2019).
- [3] F. Noé and E. Rosta, *Markov Models of Molecular Kinetics*, *J Chem Phys* **151**, (2019).
- [4] B. E. Husic and V. S. Pande, *Markov State Models: From an Art to a Science*, *J Am Chem Soc* **140**, 2386 (2018).
- [5] S. Bajpai, B. K. Petkov, M. Tong, C. R. A. Abreu, N. N. Nair, and M. E. Tuckerman, *An Interoperable Implementation of Collective-variable Based Enhanced Sampling Methods in Extended Phase Space within the OpenMM Package*, *J Comput Chem* **44**, 2166 (2023).
- [6] G. M. Torrie and J. P. Valleau, *Nonphysical Sampling Distributions in Monte Carlo Free-Energy Estimation: Umbrella Sampling*, *J Comput Phys* **23**, 187 (1977).
- [7] W. E. W. Ren, and E. Vanden-Eijnden, *Finite Temperature String Method for the Study of Rare Events*, *J Phys Chem B* **109**, 6688 (2005).
- [8] E. Rosta, M. Nowotny, W. Yang, and G. Hummer, *Catalytic Mechanism of RNA Backbone Cleavage by Ribonuclease H from Quantum Mechanics/Molecular Mechanics Simulations*, *J Am Chem Soc* **133**, 8934 (2011).
- [9] J. Schlitter, M. Engels, and P. Krüger, *Targeted Molecular Dynamics: A New Approach for Searching Pathways of Conformational Transitions*, *J Mol Graph* **12**, 84 (1994).
- [10] J. M. Bello-Rivas and R. Elber, *Exact Milestoning*, *J Chem Phys* **142**, (2015).
- [11] J. Comer, J. C. Gumbart, J. Héning, T. Lelièvre, A. Pohorille, and C. Chipot, *The Adaptive Biasing Force Method: Everything You Always Wanted To Know but Were Afraid To Ask*, *J Phys Chem B* **119**, 1129 (2015).
- [12] E. Darve and A. Pohorille, *Calculating Free Energies Using Average Force*, *J Chem Phys* **115**, 9169 (2001).
- [13] A. Barducci, M. Bonomi, and M. Parrinello, *Metadynamics*, *Wiley Interdiscip Rev Comput Mol Sci* **1**, 826 (2011).
- [14] E. Darve, D. Rodríguez-Gómez, and A. Pohorille, *Adaptive Biasing Force Method for Scalar and Vector Free Energy Calculations*, *J Chem Phys* **128**, (2008).
- [15] A. Barducci, G. Bussi, and M. Parrinello, *Well-Tempered Metadynamics: A Smoothly Converging and Tunable Free-Energy Method*, *Phys Rev Lett* **100**, 20603 (2008).
- [16] G. Lazzeri, C. Micheletti, S. Pasquali, and P. Faccioli, *RNA Folding Pathways from All-Atom Simulations with a Variationally Improved History-Dependent Bias*, *Biophys J* **122**, 3089 (2023).
- [17] G. M. Rotskoff, *Sampling Thermodynamic Ensembles of Molecular Systems with Generative Neural Networks: Will Integrating Physics-Based Models Close the Generalization Gap?*, *Curr Opin Solid State Mater Sci* **30**, 101158 (2024).
- [18] N. Naleem, C. R. A. Abreu, K. Warmuz, M. Tong, S. Kirmizialtin, and M. E. Tuckerman, *An Exploration of Machine Learning Models for the Determination of Reaction Coordinates Associated with Conformational Transitions*, *J Chem Phys* **159**, (2023).
- [19] V. K. Ramaswamy, S. C. Musson, C. G. Willcocks, and M. T. Degiacomi, *Deep Learning Protein*

- Conformational Space with Convolutions and Latent Interpolations, *Phys Rev X* **11**, 011052 (2021).
- [20] Y. Wang, J. M. Lamim Ribeiro, and P. Tiwary, *Machine Learning Approaches for Analyzing and Enhancing Molecular Dynamics Simulations*, *Curr Opin Struct Biol* **61**, 139 (2020).
- [21] J. Widmer, C. Langini, A. Vitalis, and A. Caflisch, *Optimized Reaction Coordinates for Analysis of Enhanced Sampling*, *J Chem Phys* **159**, (2023).
- [22] E. Rosta and G. Hummer, *Free Energies from Dynamic Weighted Histogram Analysis Using Unbiased Markov State Model*, *J Chem Theory Comput* **11**, 276 (2015).
- [23] C. R. Schwantes and V. S. Pande, *Improvements in Markov State Model Construction Reveal Many Non-Native Interactions in the Folding of NTL9*, *J Chem Theory Comput* **9**, 2000 (2013).
- [24] A. Pérez, P. Herrera-Nieto, S. Doerr, and G. De Fabritiis, *AdaptiveBandit: A Multi-Armed Bandit Framework for Adaptive Sampling in Molecular Simulations*, *J Chem Theory Comput* **16**, 4685 (2020).
- [25] C. Wehmeyer and F. Noé, *Time-Lagged Autoencoders: Deep Learning of Slow Collective Variables for Molecular Kinetics*, *J Chem Phys* **148**, (2018).
- [26] H. Jung, R. Covino, A. Arjun, C. Leitold, C. Dellago, P. G. Bolhuis, and G. Hummer, *Machine-Guided Path Sampling to Discover Mechanisms of Molecular Self-Organization*, *Nat Comput Sci* **3**, 334 (2023).
- [27] R. B. Best and G. Hummer, *Reaction Coordinates and Rates from Transition Paths*, *Proceedings of the National Academy of Sciences* **102**, 6732 (2005).
- [28] H. Jung, K. Okazaki, and G. Hummer, *Transition Path Sampling of Rare Events by Shooting from the Top*, *J Chem Phys* **147**, (2017).
- [29] B. Narayan, Y. Yuan, A. Fathizadeh, R. Elber, and N.-V. Buchete, *Long-Time Methods for Molecular Dynamics Simulations: Markov State Models and Milestoning*, in (2020), pp. 215–237.
- [30] A. V. Sinitskiy and V. S. Pande, *Theoretical Restrictions on Longest Implicit Time Scales in Markov State Models of Biomolecular Dynamics*, *J Chem Phys* **148**, (2018).
- [31] S. Kumar, J. M. Rosenberg, D. Bouzida, R. H. Swendsen, and P. A. Kollman, *THE Weighted Histogram Analysis Method for Free-energy Calculations on Biomolecules. I. The Method*, *J Comput Chem* **13**, 1011 (1992).
- [32] L. S. Stelzl, A. Kells, E. Rosta, and G. Hummer, *Dynamic Histogram Analysis to Determine Free Energies and Rates from Biased Simulations*, *J Chem Theory Comput* **13**, 6328 (2017).
- [33] O. Blumer, S. Reuveni, and B. Hirshberg, *Stochastic Resetting for Enhanced Sampling*, *J Phys Chem Lett* **13**, 11230 (2022).
- [34] E. J. Woods and D. J. Wales, *Analysis and Interpretation of First Passage Time Distributions Featuring Rare Events*, *Physical Chemistry Chemical Physics* **26**, 1640 (2024).
- [35] A. Kells, V. Koskin, E. Rosta, and A. Annibale, *Correlation Functions, Mean First Passage Times, and the Kemeny Constant*, *J Chem Phys* **152**, (2020).
- [36] D. Berta, S. Gehrke, K. Nyíri, B. G. Vértessy, and E. Rosta, *Mechanism-Based Redesign of GAP to Activate Oncogenic Ras*, *J Am Chem Soc* **145**, 20302 (2023).
- [37] A. Kells, Z. É. Mihálka, A. Annibale, and E. Rosta, *Mean First Passage Times in Variational Coarse Graining Using Markov State Models*, *J Chem Phys* **150**, (2019).
- [38] Z. Koczor-Benda, T. Mateeva, and E. Rosta, *Direct Calculation of Electron Transfer Rates with the Binless Dynamic Histogram Analysis Method*, *J Phys Chem Lett* **14**, 9935 (2023).
- [39] R. Gasper and F. Wittinghofer, *The Ras Switch in Structural and Historical Perspective*, *Biol Chem* **401**, 143 (2019).
- [40] A. Wittinghofer, K. Scheffzek, and M. R. Ahmadian, *The Interaction of Ras with GTPase-activating Proteins*, *FEBS Lett* **410**, 63 (1997).
- [41] T. Rudack, F. Xia, J. Schlitter, C. Köttling, and K. Gerwert, *The Role of Magnesium for Geometry and Charge in GTP Hydrolysis, Revealed by Quantum Mechanics/Molecular Mechanics Simulations*, *Biophys J* **103**, 293 (2012).
-